Encapsulation of the Transition Metals Chromium through Cobalt in Zirconium Cluster Iodides

Timothy Hughbanks,[1] Guy Rosenthal, and John D. Corbett*

Contribution from the Department of Chemistry, Iowa State University, Ames, Iowa 50011.
Received August 3, 1987

Abstract: The phases $Zr_6I_{12}Cr$, $Zr_6I_{12}Mn$, $Zr_6I_{14}Fe$, $Zr_6I_{14}Co$, $CsZr_6I_{14}Mn$, $Cs_{0.63}Zr_6I_{14}Fe$, and $Cs_xZr_6I_{14}Co$ have been synthesized by reaction of Zr, ZrI_4, the appropriate transition-metal diiodide, and cesium iodide where appropriate at 750–850 °C in sealed tantalum containers. They have the structural frameworks of $Zr_6I_{12}C$ (space group $R\bar{3}$) or $CsZr_6I_{14}C$ (*Cmca*) but with the transition metal "interstitial" instead of carbon centered in the expanded zirconium octahedra. The structures of $CsZr_6I_{14}Mn$ and $Cs_{0.63}Zr_6I_{14}Fe$ were established by single-crystal X-ray diffraction methods. The zirconium–interstitial distances in the relatively large clusters are short compared with other examples, averaging 2.490 and 2.484 Å, respectively. Extended Hückel calculations for $Zr_6I_{14}Fe$ highlight the differences between transition-metal and main-group interstitial elements, the former exhibiting a preferred stability at 18 rather than 14 cluster-binding electrons through the addition of the nonbonding e_g^4 level on the interstitial. The iron–zirconium bonding in the cluster is notably greater than that in Zr_3Fe. The phase $CsZr_6I_{14}Mn$ is properly diamagnetic, while the magnetic susceptibility data for the 19-electron $Zr_6I_{12}Mn$ are well described by a high-temperature μ_{eff} of 1.84 μ_B and an intracluster spin–orbit coupling (ζ = 312 cm^{-1}) that partially quenches the moment at lower temperatures.

The synthesis of new cluster and condensed cluster compounds of the early transition and lanthanide metals has moved forward rapidly with the realization that many M_6X_{12} (X = Cl, Br, I) type cluster phases may be stabilized by the inclusion of "interstitial" atoms.[2-4] Specifically, zirconium halide clusters have been made in which main-group elements H, Be, B, C, N, Al, Si, Ge, or P are ensconced within the octahedral cavities of the metal clusters in a variety of structure types.[5-10] Experience with this chemistry indicates that compounds in which the formal cluster electron count is 14 (including the interstitial atom's electrons) tend to enjoy particular thermodynamic stability. Examples of compounds conforming to this counting rule are $Zr_6Cl_{12}Be$,[10] $Zr_6Cl_{13}B$,[5] $Zr_6Cl_{14}C$,[6] $Zr_6Cl_{15}N$,[10] $CsZr_6I_{14}B$,[7] $KZr_6Cl_{13}Be$,[5] $KZr_6Cl_{15}C$,[9] and many more. Notable exceptions to this electronic "rule" are more prevalent among iodides and include $Zr_6I_{12}C$ (16 e), $CsZr_6I_{14}C$ and $Zr_6I_{12}B$ (15 e), and $Cs_{0.35}Zr_6I_{14}P$ (35% of the clusters with 16 e).[6-8] Almost all of these clusters may be thought of as isoelectronic with the long known $(Nb,Ta)_6X_{12}^{n+}$ (n = 2–4) ions.[11,12] Indeed, several structure types exhibited by interstitially stabilized zirconium cluster compounds were originally identified for cluster compounds of transition-metal group 5.

In a recent communication we reported the development of a new branch of this cluster chemistry whereupon zirconium and rare-earth metal clusters centered by transition metals had been found.[13] Although the compounds discovered so far in this class adopt structure types identical with those of previously synthesized phases,[14] they represent a marked electronic departure from earlier cluster chemistry. This new cluster type demands a bonding picture to account for the interstitials' valence d orbitals, the presence of direct bonding between transition and cluster metals, and the fact that these clusters are invariably more electron-rich. The zirconium iodide phases discussed in the present paper all possess clusters with a formal electron count of 18 or more. We detail here our efforts concerning the synthesis, structural characterization, magnetic properties, and electronic structure of zirconium iodide cluster compounds featuring the enclosure of the transition metals Cr, Mn, Fe, and Co.

Experimental Section

Materials. The purity, preparation, and handling of reactor-grade Zr and ZrI_4 have been previously described.[15] Powdered metal was prepared by the successive hydrogenation, grinding, and dehydrogenation under high vacuum, starting with strips of the reactor-grade metal. CsI was vacuum-sublimed prior to use. MI_2 (M = Cr, Mn, Fe, Co) phases were prepared by reacting the elements in sealed silica vessels under a sufficiently steep temperature gradient so that the I_2 pressure remained less than 1 atm while the other end was hot enough to give useful reaction rates at the metals. Each of the diiodides was vacuum-sublimed two or more times prior to use. The NiI_2 was similarly prepared from the elements but sublimed in a sealed tube to avoid decomposition to the elements. Included I_2 was removed by heating at 200 °C under vacuum until iodine was no longer evolved.

Quantitative Syntheses. All reactions were run in sealed Ta tubes with use of techniques described previously.[15,16] Well-crystallized samples of $Cs_{0.63}Zr_6I_{14}Fe$, $CsZr_6I_{14}Mn$, and $Zr_6I_{12}Mn$ were obtained as single-phase products (>95% yield) by reaction of stoichiometric amounts of FeI_2 or MnI_2, ZrI_4, Zr powder (or excess Zr strips), and CsI where appropriate. Temperatures from 750 to 850 °C are effective with reaction times of 2–4 weeks.

Yields were estimated from careful analysis of X-ray powder patterns and by microscopic inspection. The above products occur mainly as gemlike, well-faceted black crystals. The cesium content of $Cs_{0.63}ZrI_{14}Fe$ and $CsZr_6I_{14}Mn$ were established by single-crystal X-ray diffraction (see below) and for the iron compound should be taken as strictly applicable only to the crystal examined since fractional occupancies are sometimes found to be variable.[6,8] Since the iron crystal was formed in a reaction loaded with a twofold excess of the amount of the CsI necessary to give full cesium occupancy, it is likely that this cesium content represents an upper limit. The diamagnetic character of $CsZr_6I_{14}Mn$ (see Results and Discussion) is consistent with the full cesium occupancy found in single-crystal X-ray studies.

Other Reactions. The phase $Cs_{0.63}Zr_6I_{14}Fe$ was first synthesized with Fe powder instead of FeI_2, but the yield of the cluster phase was only 50%

(1) Present address: Department of Chemistry, Texas A&M University, College Station, TX 77843.
(2) Warkentin, E.; Masse, R.; Simon, A. *Z. Anorg. Allg. Chem.* **1982**, *491*, 323.
(3) Simon, A.; Warkentin, E. *Z. Anorg. Allg. Chem.* **1983**, *497*, 79.
(4) Ford, J. E.; Corbett, J. D.; Hwu, S.-J. *Inorg. Chem.* **1983**, *22*, 2789.
(5) Ziebarth, R. P.; Corbett, J. D. *J. Am. Chem. Soc.* **1985**, *107*, 4571.
(6) Smith, J. D.; Corbett, J. D. *J. Am. Chem. Soc.* **1985**, *107*, 5704.
(7) Smith J. D.; Corbett, J. D. *J. Am. Chem. Soc.* **1986**, *108*, 1927.
(8) Rosenthal, G.; Corbett, J. D. *Inorg. Chem.* **1988**, *27*, 53.
(9) Ziebarth, R. P.; Corbett, J. D. *J. Am. Chem. Soc.* **1987**, *109*, 4844.
(10) Ziebarth, R. P.; Corbett, J. D., to be submitted for publication.
(11) Schäfer, H.; Schnering, H.-G. *Angew. Chem.* **1964**, *76*, 833.
(12) Wells, A. F. *Structure Inorganic Chemistry*, 5th ed.; Clarendon: Oxford, England, 1984; pp 432–437.
(13) Hughbanks, T.; Rosenthal, G.; Corbett, J. D. *J. Am. Chem. Soc.* **1986**, *108*, 8289.
(14) Recent work shows that this chemistry will indeed lead to new structure types as well: Hughbanks, T.; Corbett, J. D., unpublished research. Structure types otherwise absent from the zirconium chloride cluster systems are now also appearing in their transition-metal-centered chemistry: Zhang, J.; Hughbanks, T.; Corbett, J. D., unpublished research.
(15) Guthrie, D. H.; Corbett, J. D. *J. Solid State Chem.* **1981**, *37*, 256.
(16) Hwu, S.-J.; Corbett, J. D.; Poeppelmeier, J. R. *J. Solid State Chem.* **1985**, *57*, 43.

0002-7863/88/1510-1511$01.50/0

Table I. Lattice Constants (Å) and Cell Volumes (Å^3) for New Zirconium Iodide Cluster Phases[a]

compound[b]	a	b	c	V
$Zr_6I_{12}Cr$[c]	14.720 (6)	a	10.049 (6)	1886 (3)
$Zr_6I_{12}Mn$	14.747 (1)	a	10.094 (1)	1901.1 (3)
$CsZr_6I_{14}Mn$	16.088 (1)	14.409 (1)	13.140 (1)	3046.0 (3)
$Zr_6I_{14}Fe$	15.976 (2)	14.355 (4)	13.019 (2)	2986 (1)
$Cs_{0.63}Zr_6I_{14}Fe$	16.021 (1)	14.380 (1)	13.075 (1)	3012.3 (3)
$Zr_6I_{14}Co$	15.988 (2)	14.321 (3)	13.009 (2)	2978.8 (8)
$Cs_xZr_6I_{14}Co$	16.065 (2)	14.360 (3)	13.096 (3)	3021 (1)

[a] Dimensions and their standard deviations deduced from least-squares refinements of Guinier powder diffraction data; λ = 1.540 56 Å. [b] Zr_6I_{12} phases are isostructural with $Zr_6I_{12}C$, space group $R\bar{3}$;[6] Zr_6I_{14} types, with Nb_6Cl_{14}, space group *Cmca*.[18] [c] Poorly crystalline material that gave only a few broad lines; the standard deviation estimates may be low.

(along with ZrI_3, ZrI_2, and a trace of Cs_2ZrI_6). The ternary product $Zr_6I_{14}Fe$ was not obtained from the corresponding reaction run under comparable conditions. However, the ternaries $Zr_6I_{14}Fe$ and $Zr_6I_{14}Co$ can be prepared in 75% and 50% yield, respectively, with MI_2 (M = Fe, Co) as the source of interstitial. The most obvious side product is ZrI_3, and some ZrI_2 can be detected as well from analysis of powder diffraction films. We presume these other products arise following effective loss of iron or cobalt values, most likely by reduction of MI_2 to intermetallic phases of zirconium, since ZrI_2 (and ZrI_3) are always obtained in the absence of a workable interstitial element. The phase $Cs_xZr_6I_{14}Co$ was obtained in 80% yield from the reaction of stoichiometric ZrI_4, CsI (for x = 1), CoI_2, and excess metal at 800 °C for 22 days, the other observed product being ZrI_2. Lower temperatures worked less well. All attempts to make $Zr_6I_{14}Mn$ yielded only $Zr_6I_{12}Mn$ plus ZrI_3. Conversely, $Zr_6I_{12}Fe$ was not formed even in zirconium-rich reactions; instead, $Zr_6I_{14}Fe$ was obtained in poor yield along with greater than usual amounts of ZrI_2.

The compound $Zr_6I_{12}Cr$ was first observed in a reaction with ZrI_4, CrI_2, and excess Zr strips as reactants. Chromium was observed to have plated out on the zirconium strips, but a "6–12" pattern was detectable when the plated area was selectively scraped for a diffraction sample. When excess chromium metal is allowed to equilibrate with preformed ZrI_2[15] at 700 °C for 6 weeks, the yield of $Zr_6I_{12}Cr$ can be improved to about 60%, with side products of unreacted ZrI_2, ZrI_3, and presumably some Zr or perhaps CrI_2, though neither of the latter two materials was detected. The product was sufficiently poorly crystallized so that some of the characteristic doublets in the pattern could not be resolved.

Despite many attempts, we have been unable to synthesize any zirconium iodide cluster compounds with nickel as the interstitial. Attempts to make quaternary phases were equally unsuccessful. Our exploration of possible vanadium-centered clusters has been much less extensive, but preliminary work has not yielded any sign of their existence.

X-ray Diffraction Studies. Preliminary product identification utilized X-ray powder diffraction film data collected with a focusing Guinier camera (Enraf-Nonius) equipped with a quartz monochromator to give clean Cu Kα_1 radiation. Sample mounting has been described previously.[17] Powdered silicon (NBS, SRM-640) was included as an internal standard, and the positions of the five observed lines were fit to known diffraction angles by a quadratic function. Lattice constants for known structures were determined by standard least-squares refinements of the indexed data. Lattice constants for the new phases discovered are given in Table I.

Reaction containers were opened in a drybox, and suitable crystals were mounted under low magnification in thin-wall capillaries. Single-crystal data were collected at room temperature on a SYNTEX $P2_1$ diffractometer with monochromatized Mo Kα radiation (λ = 0.710 69 Å) and variable-scan speeds of 1.5–29.3° min^{-1}. Data collection and refinement parameters are given in Table II. Empirical absorption corrections were carried out with full-circle, ϕ-scan data measured for the manganese and iron cases at two and three values of θ, respectively. Programs used in structure refinement have been referenced previously.[16] Atomic scattering factors included corrections for contributions to anomalous dispersion.

As observed earlier with the cluster carbides,[6] secondary extinction corrections[18] had a notable effect on the refinements. Intense reflections make positive contributions to the electron density at the interstitital site in the center of the clusters in both the $Zr_6I_{12}Z$ and $Zr_6I_{14}Z$ structures,

Table II. Data Collection and Refinement Parameters

	$CsZr_6I_{14}Mn$	$Cs_{0.63}Zr_6I_{14}Fe$
space gp	*Cmca*	*Cmca*
Z	4	4
cryst dimen, mm	0.30 × 0.25 × 0.20	0.2 × 0.2 × 0.15
2θ(max), deg	55	55
no. of reflcns		
measured	3775	3727
observed[a]	2377	1884
independent	1295	1050
R(av), %	2.9	1.9
abs coeff μ, cm^{-1} (Mo Kα)	175	181
range of tranmissn coeff (normalized)	0.37–1.0	0.63–1.0
second ext coeff (10^{-4})	0.25 (1)	0.10 (1)
R,[b] %	3.1	3.6
R_w,[c] %	3.7	4.5
no. of variables	59	60

[a] $F_o \geq 3\sigma_F$ and $I_o > 3\sigma_I$. [b] $R = \sum(|F_o| - |F_c|)/\sum|F_o|$. [c] $R_w = [\sum w(|F_o| - |F_c|)^2/\sum w|F_o|^2]^{1/2}$.

and a systematic error such that $F_o < F_c$ produces the corresponding electron density error. (The interstitial atom Z may be thought of as sitting on a vacant site of the close-packed iodine sublattice that runs through both the $M_6I_{12}Z$ and $M_6I_{14}Z$ structure types. This iodine sublattice causes a subset of the reflections corresponding the "reciprocal sublattice" to be the most intense in these systems.) Well-formed, gem-like crystals were used in data collections, and the inclusion of secondary extinction corrections typically resulted in a drop in the residuals of a few percent.

Initial positions for the heavy atoms in each case were taken from data obtained earlier for compounds with light-atom interstitials.[6,7] For the $Cs_{0.63}Zr_6I_{14}Fe$ compound, the refinement was first carried through without any atom in the cluster center, the residual R thereby decreasing to 9%. A Fourier map showed a peak in the center of the cluster that corresponded to an atom with $Z \cong 23$–26, the value depending on which iodine was used as a basis for comparison. Inclusion of the iron and subsequent full-matrix refinement with the iron occupancy set to unity gave a satisfactory solution (upon which the parameters reported in the tables are based). When the iron occupancy and isotropic thermal parameters were simultaneously varied, the occupancy dropped to 91 (2)% and B shrank to 0.7 (1). In $CsZr_6I_{14}Mn$, the manganese occupancy similarly refined to 94 (1)%. Since the final difference maps calculated with the interstitial occupancies set to unity did not show any significant peaks (<0.5 e/Å^3 and not near Fe or Mn), we doubt the significance of these small departures from full occupancy. Lattice constants deduced from different preparations were sufficiently invariant to suggest that admixed interstitials from impurities were not a problem either. The cesium site occupancies were also varied, giving values of 63 (1)% and 98.0 (5)% for the iron and manganese compounds, respectively. The latter was returned to unity for the final refinement cycles.

Extended Hückel Calculations. The molecular orbital description given subsequently derives from extended Hückel calculations on a $(Zr_6I_{18}Fe)^{4-}$ cluster, the unit that includes the six, structurally important iodine atoms terminal to the cluster's vertices. While the cluster calculation was of the noniterative variety, the valence state ionization potentials (H_{ii} values) used were taken from an iterative band calculation on a (neutral) model $Zr_6I_{14}Fe$ system with one cluster per unit cell. This iterative calculation was necessary in order to establish reasonable relative energies for the d orbitals of zirconium and iron in this kind of compound. Noniterative calculations using previously published H_{ii} values for these metals put a large and unreasonably negative charge on the iron (~−3). This kind of anomalous behavior has been previously noted in moving to condensed metal–metal bonded surface systems with parameter sets suitable for organometallic species.[20] Parameters used in the present study are available as supplementary material.

Magnetic Susceptibilities. Static data for $CsZr_6I_{14}Mn$ and $Zr_6I_{14}Mn$ were secured between 2.6 and 350 K with a commercial SQUID magnetometer (Quantum Design, Inc., San Diego, CA).

Results and Discussion

Most zirconium cluster iodides containing an interstitial transition metal M may be obtained from fairly direct reactions of Zr, ZrI_4, and MI_2 in sealed tantalum containers at 750–850 °C. The phases reported here (Table I) and their cluster-based electron counts are $Zr_6I_{12}Cr$ (18), $Zr_6I_{12}Mn$ (19), $CsZr_6I_{14}Mn$ (18),

(17) Daake, R. L.; Corbett, J. D. *Inorg. Chem.* **1978**, *17*, 1192.
(18) Simon, A.; von Schnering, H.-G.; Wöhrle, H.; Schäfer, H. *Z. Anorg. Allg. Chem.* **1965**, *339*, 155.
(19) Coppens, P.; Hamilton, W. C. *Acta Crystallogr., Sect. A: Cryst. Phys., Diffr., Theor. Gen. Crystallogr.* **1970**, *A26*, 7.
(20) Saillard, J.-Y.; Hoffmann, R. *J. Am. Chem. Soc.* **1984**, *106*, 2006.

Table III. Final Positional Parameters for $CsZr_6I_{14}Mn$ and $Cs_{0.63}Zr_6I_{14}Fe$

	$CsZr_6I_{14}Mn$			$Cs_{0.63}Zr_6I_{14}Fe$		
	x	*y*	*z*	*x*	*y*	*z*
Zr1	0.38893 (5)	0.06787 (5)	0.88813 (6)	0.38890 (8)	0.0674 (1)	0.8875 (1)
Zr2	0	0.35905 (7)	0.89631 (9)	0	0.3587 (1)	0.8963 (2)
I1	0.12539 (3)	0.08882 (3)	0.24910 (5)	0.12535 (6)	0.08953 (5)	0.24881 (8)
I2	0.12572 (3)	0.25484 (4)	0.00548 (4)	0.12565 (6)	0.25504 (7)	0.00648 (8)
I3	0.25	0.34634 (5)	0.25	0.25	0.3471 (1)	0.25
I4	0	0.16061 (5)	0.75993 (6)	0	0.1591 (1)	0.7625 (1)
I5	0.24708 (5)	0	0	0.24639 (8)	0	0
Cs[a]	0	0	0	0	0	0
Mn, Fe	0.5	0.5	0.5	0.5	0.5	0.5

[a] Refined cesium multiplicity in iron phase, 0.63 (1).

Table IV. Important Bond Lengths in $Cs_xZr_6I_{14}Z$ Phases[a]

	frequencies	$CsZr_6I_{14}Mn$	$Cs_{0.63}Zr_6I_{14}Fe$	$CsZr_6I_{14}B$	$CsZr_6I_{14}C$	$Cs_{0.7}Zr_6I_{14}Al$	$Cs_{0.3}Zr_6I_{14}Si$	$Cs_{0.35}Zr_6I_{14}P$
Zr–Zr								
intralayer[b]								
Zr1–Zr1	2	3.574 (2)	3.560 (3)	3.414 (2)	3.324 (2)	3.462 (5)	3.632 (4)	3.544 (2)
Zr1–Zr2	4	3.502 (1)	3.493 (2)	3.349 (2)	3.257 (2)	3.408 (4)	3.562 (3)	3.468 (2)
interlayer								
Zr1–Zr1	2	3.531 (2)	3.524 (3)	3.390 (2)	3.321 (2)	3.444 (5)	3.574 (4)	3.510 (2)
Zr1–Zr2	4	3.511 (1)	3.505 (2)	3.357 (2)	3.270 (2)	3.391 (4)	3.574 (3)	3.498 (2)
Zr–interstitial								
Zr–int	4	2.512 (1)	2.505 (1)	2.406 (1)	2.349 (1)	2.442 (3)	2.548 (2)	2.494 (1)
Zr–int	2	2.446 (1)	2.443 (2)	2.335 (2)	2.265 (1)	2.356 (4)	2.498 (3)	2.432 (2)
av		2.490	2.484	2.382	2.321	2.413	2.531	2.473
Zr–I								
Zr–I^i(av)		2.893 (1)	2.901 (2)	2.889 (1)	2.874 (1)	2.884 (3)	2.893 (2)	2.879 (1)
Zr–I^{i-a}	4	2.960 (1)	2.958 (2)	2.933 (1)	2.920 (1)	2.932 (3)	2.957 (3)	2.951 (1)
Zr–I^{a-i}	2	3.374 (1)	3.361 (2)	3.421 (1)	3.522 (2)	3.405 (5)	3.256 (4)	3.324 (2)
Zr–I^{a-a}	4	3.133 (1)	3.113 (1)	3.177 (1)	3.195 (1)	3.137 (3)	3.068 (2)	3.090 (1)
Cs–I	4	4.052 (1)	4.034 (1)	4.011 (1)	4.010 (1)	4.007 (2)	3.998 (1)	3.986 (1)
	4	4.193 (1)	4.184 (1)	4.163 (1)	4.185 (1)	4.168 (2)	4.149 (1)	4.163 (1)
	2	3.912 (1)	3.857 (1)	3.860 (1)	3.837 (1)	3.826 (3)	3.808 (2)	3.769 (1)
	2	3.975 (1)	3.947 (1)	3.953 (1)	3.914 (1)	3.932 (3)	3.948 (2)	3.926 (1)

[a] Other data from ref 6–8. [b] Layers lie normal to $\vec{c}$, Figure 1.

$Zr_6I_{14}Fe$ (18), $Cs_{0.63}Zr_6I_{14}Fe$ (18.6), $Zr_6I_{14}Co$ (19), and $Cs_xZr_6I_{14}Co$ ($19 + x$). The two manganese compounds and the quaternary cesium–iron example were obtained as well-faceted crystals in virtually quantitative yield, while the others were made mainly as powders and in lesser yields. The principal side reaction is thought to be loss of the transition metal by reaction of MI_2 with zirconium metal. In the case of chromium, the best yield (~60%) of a poorly crystalline $Zr_6I_{12}Cr$ was attained by direct reaction of the layered[15] ZrI_2 with excess chromium at 700 °C.

The $Zr_6I_{12}M$ phases occur in the $Zr_6I_{12}C$ structure type,[6] while $Zr_6I_{14}M$ structures, already known for $Zr_6Cl_{14}B$,[5,10] $Zr_6I_{14}C$,[6] $Zr_6I_{14}Si$,[7] and others, have the long-known structural framework of Nb_6Cl_{14}[18] where the cluster is empty. The cesium examples of the latter structure type reported here and elsewhere[5-8] in effect amount to a second kind of interstitial derivative of the Nb_6Cl_{14} structure in which cesium (or another alkali metal) is bound between clusters and has only halogen neighbors.

Crystal Structures. The structures of the quaternary manganese and iron-containing clusters were refined by single-crystal X-ray diffraction on crystals with the compositions $CsZr_6I_{14}Mn$ and $Cs_{0.63}Zr_6I_{14}Fe$, respectively. Atomic coordinates and their standard deviations are compiled in Table III; anisotropic thermal parameters and the observed and calculated structure factor amplitudes for each are available as supplementary material. Table IV contains important bond lengths for these two structures along with those from previous work on related $Cs_xZr_6I_{14}Z$ phases for the purpose of comparison. Figure 1 contains ORTEP drawings of $Cs_{0.63}Zr_6I_{14}Fe$: (top) an individual cluster together with terminal iodines; (bottom) the complete cell illustrating the intercluster iodine bridging.

In subsequent discussions we employ the following notation to describe the bonding roles of the iodines (i = inner; a = outer): I^i, for iodines that edge bridge a metal cluster under consideration; I^a, for iodines that fill the exo positions on the cluster vertices and thus participate in one of the six radial Zr–I bonds that each cluster demands; I^{i-a}, for an iodine that is edge-bridging on the cluster under examination and exo-bonded to an adjacent cluster; I^{a-i}, for iodine exo-bonded to the cluster in question, edge-bridging on an adjacent cluster; I^{a-a}, for the atom exo-bonded to two adjacent clusters, thereby linking them together.

Both the $Zr_6I_{12}Z$ and $M^IZr_6I_{14}Z$ (Z = interstitial atom, M^I = alkali metal or nothing) structure types have been previously described.[6] The $Zr_6I_{12}Z$ structure consists of octahedral zirconium clusters that are slightly compressed trigonally and centered by an interstitial Z. The metal polyhedra with all edges bridged by iodines (I^i) are cubic close-packed into a rhombohedral array without any intervening iodides. The cluster orientations are such that iodines on adjacent clusters bond at exo positions (I^a) about the zirconium atoms of the cluster in question, and vice versa. The cluster bonding requirements are similarly satisfied in $M^IZr_6I_{14}Z$ structures (Figure 1) except that each $Zr_6I_{12}Z$ unit is now bound to four iodines that are instead equally shared by two clusters apiece (I^{a-a}). As shown, these linking iodines help stitch the three-dimensional network of clusters together and add 4/2 more iodines per cluster to the compound to give a phase with a Zr:I ratio of 6:14. The other two cluster vertices are still bonded to inner iodines (I^{i-a}) in another unit. The M^I atom, if any, resides in a 12-coordinate site surrounded by iodines; collectively, the M^I atoms, iodines, and Z atoms form close-packed layers that are stacked in a ···ABCB··· fashion normal to the *c*-axis, which lies vertical in Figure 1.

Table IV includes only a partial list of independent bond lengths. In particular, the collection of Zr–I^i distances to iodines that are not involved in intercluster bonding are listed as the average as these vary only modestly from compound to compound. The range of Zr–I^{i-a} distances over the compounds is also only 0.04 Å, or twice as large as for Zr–I^i, and it is therefore quite reasonable to describe all of the clusters' inner iodine atoms as "riding" the

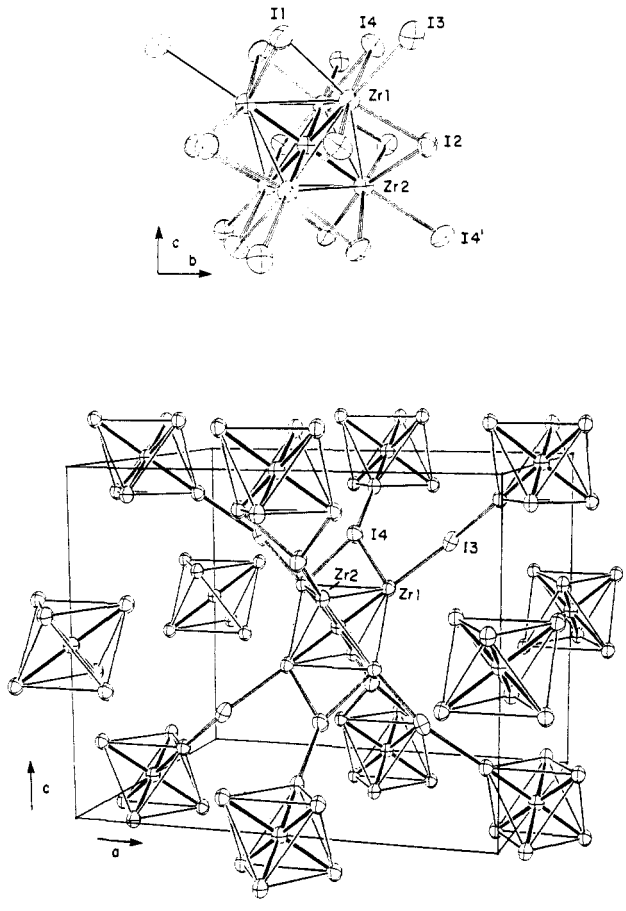

Figure 1. Structure of $Cs_{0.63}Zr_6I_{14}Fe$: (top) isolated cluster together with bridging iodines (a mirror plane in the plane of the paper contains Zr2, I4, and Fe); (bottom) unit cell showing the four $I3^{a-a}$ atoms that bridge between cluster vertices plus the two edge-bridging $I4^{a-i}$ atoms in other clusters that occupy two vertices and vice versa (I^{i-a}). The other 10 I^i (1, 2, 5) atoms that only bridge cluster edges have been omitted for clarity (90% probability thermal ellipsoids).

edges of the metal cluster as it breathes to accommodate interstitials of varying size.

The strongest influence on $Zr-I^{a-i}$ and $Zr-I^{a-a}$ distances is the effective size of the interstitial atoms. Both the d(Zr–Z) and d(Zr–Zr) data in Table IV indicate that we may order the interstitials according to size: Si > P ~ Mn ~ Fe > Al > B > C. At the same time the lengths of the $Zr-I^{a-i}$ and $Zr-I^{a-a}$ bonds act in opposition and *increase* for the successive members of approximately the same series, that is, for increasingly smaller Z atoms. We interpret this trend as a clear manifestation of the matrix effect that is particularly evident in examining iodine cluster compounds with a number of iodine–iodine contacts around the cluster. Thus when the Zr_6 octahedron expands to accommodate a larger interstitial, each metal vertex moves closer to the plane defined by the four neighboring I^i atoms. This in turn allows the exobonded iodines, which at least for small Z also ride on the inner iodine atoms, to approach closer to the zirconium atoms to which they are bonded. The cesium occupancy also has some effect on these distances via the accompanying increase in the I^{a-i} coordination number and, perhaps, because a greater intercluster separation is required to make room for cesium ions, at least for Z = C, Si, Fe, and Co according to the comparative cell volumes of $Zr_6I_{14}Z$ and $Cs_xZr_6I_{14}Z$ types. The shorter and presumably stronger $Zr-I^{a-a}$ bonds would appear to be less plastic than $Zr-I^{a-i}$, judging from their smaller range. It is also true that I^{a-a} atoms are only two-coordinate (no Cs neighbors) in all $M^I_xZr_6I_{14}Z$ compounds and would, therefore, be expected to participate in stronger Zr–I bonding.

Certainly, the most remarkable feature of the new transition-metal-centered clusters is the metal–metal bonding within the clusters. While iron and manganese are clearly large interstitials,

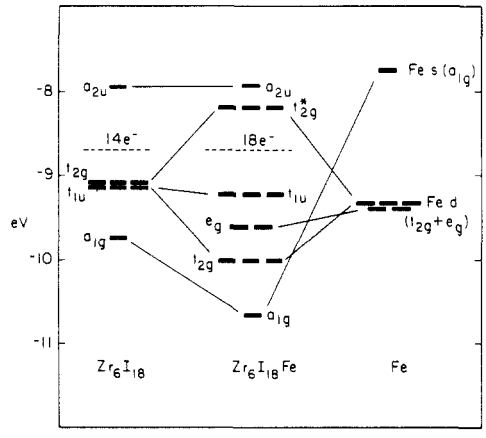

Figure 2. Energy levels for Zr–Zr bonding orbitals (left), the AO levels for iron (right), and the resulting cluster orbitals in $[Zr_6I_{12}Fe]I_6^{4-}$. A t_{1u}^6 HOMO orbital corresponds to 18 cluster-based electrons.

the Zr–Si distances in $Cs_{0.3}Zr_6I_{14}Si$[7] show silicon to be even larger. (However, relatively longer bridging iodine distances give the iron derivative the larger cell volume.) Also, the observed Zr–Fe distances (av. 2.48 Å) are notably shorter than observed in binary Zr_3Fe (av 2.63 Å) wherein the iron atoms are also six-coordinate.[21] Indeed, we are not aware of any compounds, molecular or solid-state, that exhibit Zr–Fe or Zr–Mn distances as short as found within these clusters. (Research under way has shown that transition-metal-centered zirconium chloride clusters have even shorter Zr–M distances;[14] this trend is consistent with earlier comparisons between iodide and chloride cluster compounds and a probable matrix effect.)

In previous work, it has been useful to highlight unusual features of zirconium–interstitial bonding by defining effective radii for the interstitial atoms. Using the crystal radius[22] of six-coordinate Zr^{4+} (0.86 Å), we obtain r_{Fe} = 1.62 Å and r_{Mn} = 1.63 Å. Since, as we have seen, the corresponding bond lengths in intermetallics are considerably greater than in these cluster compounds, these radii will probably be most useful in comparing zirconium iodide cluster data with those obtained for recently synthesized compounds such as $LiZr_6Cl_{15}Fe$, $Li_2Zr_6Cl_{15}Mn$,[14] $Zr_6Br_{14}Fe$,[10] and M_7I_{12}(Fe, Mn) [M = Y, Gd, Pr].[13,23] For example, the crystal radius of six-coordinate Y^{3+} is 1.04 Å, and the Y–Fe distance in $Y_7I_{12}Fe$ is 2.62 Å, yielding a slightly smaller effective radius for iron in this compound, 1.58 Å. Of course, these numbers represent largely arbitrary ways of subdividing distances, and the use of crystal radii in the description of metal–metal bonded systems in particular can at best only reflect size *trends* for the atoms involved.

Electronic Structure and Bonding. Better understanding of the bonding within these clusters comes with examination of the metal-based MO's. A diagram showing the interaction of iron atomic orbitals with those of the surrounding cluster is presented in Figure 2 according to the results of an extended Hückel calculation on an isolated $[Zr_6I_{12}Fe]I_6^{4-}$ cluster.

At the left in the figure are the metal-based levels for the empty Zr_6I_{18} cluster, already expanded in preparation for the encapsulation of the iron atom. Even with the cluster so distended, the level structure retains the essential features of such Zr_6X_{12} systems: seven orbitals with significant metal–metal bonding character fall immediately below a gap of ~1 eV. This pattern persists in main-group-centered clusters,[6,7,10,24] but in those cases, the a_{1g} and t_{1u} levels strongly interact with the central atom's s (a_{1g}) and p (t_{1u}) orbitals to form bonding and antibonding combinations. (Of course, the character of the occupied a_{1g} and t_{1u} levels changes to metal–interstitial bonding.) The antibonding orbitals are pushed

(21) Buschow, K. H. J. *J. Less-Common Met.* **1981**, *79*, 243. Distances in Zr_3Fe were calculated from the refined coordinates for Zr_3Co.
(22) Shannon, R. D. *Acta Crystallogr., Sect. A: Cryst. Phys., Diffr., Theor. Gen. Crystallogr.* **1976**, *A32*, 751.
(23) Hughbanks, T.; Corbett, J. D., submitted for publication.
(24) Hwu, S.-J.; Corbett, J. D. *J. Solid State Chem.* **1986**, *64*, 331.

well above the gap in the process, and the number of levels below the gap remains at 7, indicating a preference for 14-electron cluster configuration, as observed.

The interaction with transition metals is different: now the strongest mixing occurs in the t_{2g} ($d\pi$) and a_{1g} (s) orbital pairs while the cluster-based t_{1u} (p) and the e_g ($d\sigma$) orbitals are respectively localized on the zirconium and iron centers and much less perturbed. The splitting of the t_{2g} orbitals ($t_{2g} - t_{2g}^* \sim 2$ eV) reflects an appreciable Zr–Fe d–dπ interaction, as illustrated in **1** for one partner in each of these MO's. The iron s orbital

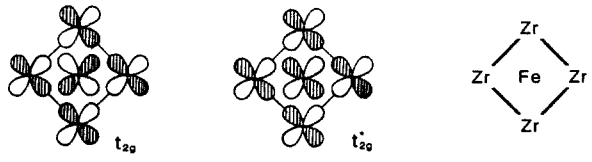

1

participates in a strong Zr–Fe σ interaction as a result of excellent overlap and a moderately good energy match with the Zr_6 a_{1g} combination (**2**). The iron p orbitals lie much higher in energy

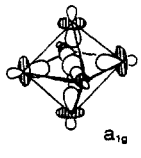

2

and mix only slightly with the t_{1u} combination in the zirconium cluster so that only 7.4% of the electron density in the resulting t_{1u} orbitals resides in the Fe p orbitals. In contrast, the iron contributions to the aforementioned orbitals are the following: t_{2g}, 41% d; t_{2g}^*, 54% d; a_{1g}, 25% s. The significant new feature is that iron e_g ($d\sigma$) orbitals do not interact strongly with the surrounding zirconium cage. Although these orbitals are clearly well directed for overlap with the zirconium-based atomic orbitals, the nearest Zr_6 combinations of e_g symmetry are high-lying. The iron e_g set is, therefore, mostly *nonbonding*, and most importantly, its presence means that the bonding–antibonding gap falls at the 18-electron level rather than at 14-electron level where it did with main-group (s, p) element interstitials.

Overlap populations for the metal–metal bonds within the cluster are in correspondence with expectations: for the 18-electron cluster, we calculate values of 0.45 for the Zr–Fe bonds and 0.17 for the relatively long Zr–Zr bonds. While these values indicate the relative importance of Zr–Fe vs Zr–Zr bonding in the cluster, more insight into the special character of Zr–Fe bonding can be gained by comparison with that in the binary intermetallic Zr_3Fe, where this role might superficially be expected to be similar. We choose this system for comparison because the Fe coordination number is approximately 6 (see **3**; the iron atom sits in a bicapped

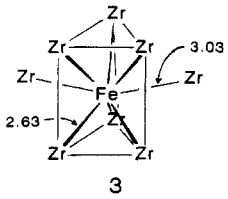

3

trigonal prism, d(Zr–Fe) = 2.63 Å, with two more distant zirconium Zr neighbors at 3.03 Å). Also, Zr_3Fe is zirconium-rich, and so the iron atom is surrounded only by zirconium; the structure is simple enough (Re_3B-type) to allow a full band structure calculation for comparison of the electronic structures. The most important computational result concerning Zr–Fe bonding is that the Zr–Fe overlap population is only 0.19 for the short (2.63 Å) contacts shown in **3**. The value is approximately half the value we obtain for the cluster iodide *even when we expand the size of the cluster* so that the Zr–Fe distance is also 2.63 Å. Further analysis of the Zr_3Fe case shows that this reduced bonding cannot

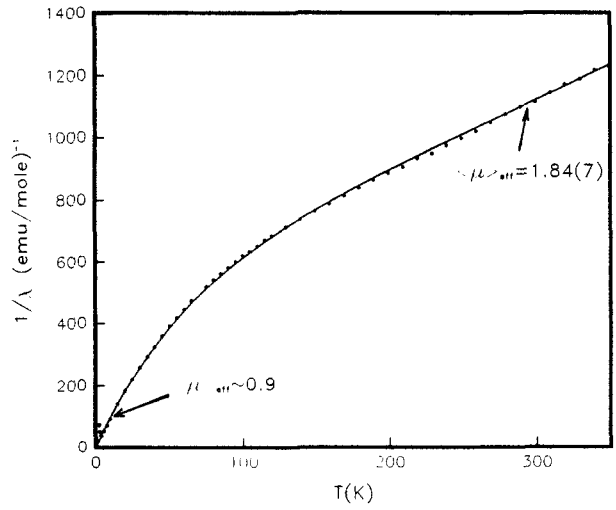

Figure 3. Inverse molar magnetic susceptibility vs temperature (K) for $Zr_6I_{12}Mn$. The μ_{eff} values shown are the limiting values at low and high temperatures. The solid curve is the result of a "Kotani fit" with a spin–orbit coupling constant of 312 cm^{-1} and an orbital reduction factor of 0.318.[28]

be the result of a misplacement of the Fermi level relative to Zr–Fe bonding and antibonding bands; the COOP (crystal orbital overlap population) curves[25] show that the Fermi level neatly separates bonding and antibonding levels for the Zr–Fe bonds. Indeed, for this structure type, the Zr–Fe bonding appears to be "optimized". The analogy carries further: A comparable Zr_6Fe unit occurs in Zr_5Sb_3Fe[26] and the Zr–Fe overlap populations at a fixed distance in fact increase through the series Zr_3Fe, Zr_5Sb_3Fe, $Zr_6I_{14}Fe$ as the zirconium–zirconium interactions diminish, the zirconium framework is oxidized, and electron density is increasingly transferred to the non-metal sheathing about the Zr_6Fe units.

The above discussion implies that 18-electrons clusters carry some extra stability and that the synthesis of such compounds should be preferred. While to some extent we believe this viewpoint to be valid, some caveats should be highlighted. The new compounds $Zr_6I_{12}Mn$, $Cs_{0.63}Zr_6I_{14}Fe$, $Zr_6I_{14}Co$, and $Cs_xZr_6I_{14}Co$ are thermally quite stable, yet these have 19, 18.6, 19, and 19 + x electrons, respectively. For manganese to form a ternary compound with 18-electrons clusters, clearly one would have to find a zirconium iodide phase with other than a 6–12 or 6–14 structure type. Such a phase has not yet appeared in investigation of either main-group- or transition-metal-centered zirconium iodide cluster compounds, in contrast to the behavior of the chlorides.[5,10] There is no fully adequate explanation for this situation, although many sublte factors are important to phase stability. Still, it is worth noting that 20-electron clusters have not been found; $Zr_6I_{12}Fe$ and $Zr_6I_{14}Ni$ have not been synthesized, and the Cs content in $Cs_xZr_6I_{14}Co$ is probably well below unity. The same "18-electron stability" seems to work against the potential 17-electron examples $Zr_6I_{14}Mn$ and $CsZr_6I_{14}Cr$. The fact that alkali-metal cations appear to stabilize quaternary compounds (presumably by increasing their lattice energies) is also not new. In the main-group cases, several iodide clusters with greater than 14 electrons can also be made using this strategy, e.g., $CsZr_6I_{14}C$, $Cs_{0.3}Zr_6I_{14}Si$, and $Cs_{0.6}Zr_6I_{14}P$.[6-8]

Magnetic Susceptibilities of the Manganese Clusters. The electronic structure scheme discussed in the previous sections carried with it the implication that 18-electron clusters should be closed shell and, therefore, diamagnetic. Since we were able to prepare the stoichiometric compound $CsZr_6I_{14}Mn$ is essentially quantitative yield, we were able to test this assertion. The phase

(25) COOP curves are introduced in: Hughbanks, T.; Hoffmann, R. *J. Am. Chem. Soc.* **1983**, *105*, 3528. See also: Wijeyesekera, S. D.; Hoffmann, R. *Organometallics* **1984**, *3*, 949. Kertesz, M.; Hoffmann, R. *J. Am. Chem. Soc.* **1984**, *106*, 3453.

(26) In Zr_5Sb_3Fe (Mn_5Si_3-type), the iron is six-coordinate trigonal antiprismatic and the Zr–Fe distances are 2.653 (2) Å. Garcia, E.; Corbett, J. D., to submitted for publication.

is diamagnetic for $T \gtrsim 8$ K. Measurements from there to 2 K showed a very small Curie tail, attributable to traces of paramagnetic impurities or to very small cesium nonstoichiometry in the major phase.

Figure 3 shows the temperature dependence of the inverse molar susceptibility (χ^{-1}) measured for the more interesting 19-electron cluster compound $Zr_6I_{12}Mn$. The high-temperature data ($T \geq 150$ K) are simplest to interpret: χ^{-1} is linear in T, and a fit of the data to Curie–Weiss expression gives an effective moment (μ_{eff}) of 1.84 (7) μ_B with a Weiss constant (Θ) of −174 (17) K. The data plotted are not "corrected" for diamagnetism since temperature-independent paramagnetic (van Vleck) contributions are apparently such that they cancel the diamagnetism; the plot is quite linear in the high-temperature regime where the χ^{-1} curve will be *most* sensitive to a temperature-independent contribution. The effective moment is consistent with the spin-only magnetism expected for clusters with one unpaired spin each.

In the range between 150 and 10 K the effective moment per cluster gradually declines to $\sim$0.9 μ_B as the temperature drops. Extrapolation of the data gives an intercept with the temperature axis quite close to 0 K. (Data below 8 K do show an upturn in χ^{-1}, presumably resulting from a very weak antiferromagnetic interaction between the clusters.) While quenching of the moment is evident as high as $\sim$130 K, no ordering temperature is observed. All of this points to an *intra*cluster mechanism as responsible for the declining effective moment at lower temperature.[27]

The susceptibility data have a natural interpretation in light of the orbital picture presented above. This 19-electron system should have a $^2T_{2g}$ ground state (arising from the $(a_{1g})^2(t_{2g})^6(e_g)^4(t_{1u})^6(t_{2g}^*)^1$ configuration) in the octahedral limit, and this will be split by spin–orbit coupling. The solid curve shown on Figure 3 represents a fit of the susceptibility data to an expression derived for a $^2T_{2g}$ ion that is of the form

$$\chi^{-1} = \left[\frac{9(2+y)}{30(k-1)^2 + 3(2k+1)^2y + 8(k+2)(1-y)x}\right]\frac{3k_BT}{N_A\mu_B^2}$$

where $y = \exp(-3\zeta_{eff}/k_BT)$ and $x = k_BT/\zeta_{eff}$. In this expression ζ_{eff} is the effective spin–orbit coupling constant, k is the "orbital reduction factor",[28] and the term in brackets is equal to μ_{eff}^{-2}. The curve shown corresponds to that for $\zeta_{eff} = 312$ cm^{-1} and $k = 0.318$.

The rate at which the curvature changes with temperature is mostly determined by ζ_{eff}. The value obtained is reasonable even when the delocalized nature of the cluster bonding is allowed for. To a good approximation, the t_{2g}^* molecular orbitals (in real form) can be expressed as

$$\Phi_{xy} = N\left\{\phi_{xy}(\mathrm{Mn}) + \frac{\lambda_{Zr}}{2}[\phi_{xy}(\mathrm{Zr1}) + \phi_{xy}(\mathrm{Zr2}) + \phi_{xy}(\mathrm{Zr3}) + \phi_{xy}(\mathrm{Zr4})]\right\}$$

where $\lambda_{Zr} > 0$ and Zr1–Zr4 lie on the xy basal plane of the octahedral cluster (see **1**). Expressions for Φ_{xz} and Φ_{yz} are analogous. From MO's of this form, one can derive the relation $\zeta_{eff} = N^2[\zeta_{Mn} + (\lambda_{Zr}^2/2)\zeta_{Zr}]$. While the precise values appropriate for ζ_{Mn} and ζ_{Zr} in the present chemical environment are uncertain, they are of the correct magnitude to yield $\zeta_{eff} = 312$ cm^{-1}.

The physical interpretation of the orbital reduction factor k is more ambiguous. In conventional treatments of single magnetic ions, it accounts for the lowering of the orbital contribution to the magnetic moment because of delocalization onto the surrounding ligands. As such, deviations from unity should be small to moderate depending on the extent of delocalization. In the metal cluster, delocalization is extensive and the deviation of the orbital reduction factor from unity will be larger. Still, the value obtained (0.318) is less than expected. A number of mechanisms may be responsible for the relatively small orbital contribution: (i) The cluster with its iodine bridging to neighboring clusters is actually trigonal, though deviations from octahedral symmetry are probably small. When the effect of the "trigonal field" is of the same order as the spin–orbit coupling energy, the orbital contribution to the magnetic moment will be reduced. (ii) When the trigonal field is left aside, the Γ_8 (G) symmetry ground state should be Jahn–Teller unstable, and the effects of dynamic distortion may be responsible for the smaller than expected orbital reduction factor. (iii) The effects of second-order mixings because of spin–orbit coupling have been neglected in our discussion, but speculation about their role on the basis of susceptibility measurements alone becomes pointless.

Acknowledgment. The authors wish to express their appreciation to Dr. D. Dudis for his help in crystallography and to Professor R. A. Jacobson for making crystallographic equipment available to us. We also thank Professor R. N. Shelton of the Iowa State University Physics Department of his assistance in collecting the magnetic susceptibility data. This research was supported by the National Science Foundation through Solid State Chemistry Grant DMR-8318616 and was carried out in the facilities of the Ames Laboratory, DOE.

Supplementary Material Available: Tables of anisotropic thermal parameters for $Cs_{0.63}Zr_6I_{14}Fe$ and $CsZr_6I_{14}Mn$ and extended Hückel orbital parameters (3 pages); listings of observed and calculated structure factor data (9 pages). Ordering information is given on any current masthead page.

(27) Our data are reminiscent of those for niobium iodide clusters in which a different intracluster mechanism (high–low spin crossover) is responsible for quenching the moment. Finley, J. J.; Camley, R. E.; Vogel, F. E.; Zevin, V.; Gmelin, E. *Phys. Rev. B: Condens. Matter* **1981**, *24*, 1023. Imoto, H.; Simon, A. *Inorg. Chem.* **1982**, *21*, 308.

(28) (a) Kotani, M. *J. Phys. Soc. Jpn.* **1949**, *4*, 293. (b) Ballhausen, C. J. *Molecular Electronic Structures of Transition Metal Complexes*; McGraw-Hill: New York, 1977; Chapter 3. (c) Abragam, A.; Bleaney, B. *Electron Paramagnetic Resonance of Transition Ions*; Dover: New York, 1986; Chapter 20.